Radiopharmaceuticals

4

David J. Yang, Tomio Inoue, and E. Edmund Kim

Radiolabeled Ligands

Several imaging modalities including computed tomography (CT), magnetic resonance imaging (MRI), ultrasound, optical imaging, and gamma scintigraphy have been used to diagnose cancer. Although CT and MRI provide considerable anatomic information about the location and the extent of tumors, they do not adequately differentiate residual or recurrent tumors from edema, radiation necrosis, or gliosis. Ultrasound images provide information about local and regional morphology with blood flow. Although optical imaging showed promising results, its ability to detect deep tissue penetration was not well demonstrated. Radionuclide imaging modalities such as positron emission tomography (PET) and single photon emission computed tomography (SPECT) are diagnostic cross-sectional imaging techniques that map the location and concentration of radionuclide-labeled compounds [1–3]. Beyond showing precisely where a tumor is and its size, shape, and viability, PET and SPECT are making it possible to "see" the molecular makeup of the tumor and its metabolic activity. Whereas PET and SPECT can provide a very accurate picture of metabolically active areas, their ability to show anatomic features is limited. As a result, new imaging modalities have begun to combine PET and SPECT images with CT scans for treatment planning. PET/CT and SPECT/CT scanners combine anatomic and functional images taken during a single procedure, without having to reposition the patient between scans. To improve the diagnosis, prognosis, planning, and monitoring of cancer treatment, characterization of tumor tissue is extensively determined by development of more tumor-specific pharmaceuticals. Radiolabeled ligands as well as radiolabeled antibodies have opened a new era in scintigraphic detection of tumors and have undergone extensive preclinical development and evaluation.

Glucose Transport

^{18}F-fluorodeoxyglucose (FDG) PET has been used to diagnose and stage tumors [4–14], myocardial

D.J. Yang, Ph.D. (✉)
Department of Experimental Diagnostic Imaging, The University of Texas MD Anderson Cancer Center, Houston, TX 77030, USA
e-mail: dyang@mdanderson.org

T. Inoue, M.D., Ph.D.
Department of Radiology, Yokohama City University Graduate School of Medicine, Yokohama 236-0004, Japan
e-mail: tomioi@yokohama-cu.ac.jp

E.E. Kim, M.D., M.S.
Departments of Nuclear Medicine and Diagnostic Radiology, The University of Texas MD Anderson Cancer Center and Medical School, Houston, TX 77030, USA

Graduate School of Convergence Science and Technology, Seoul National University, Seoul, South Korea
e-mail: ekim@mdanderson.org

E.E. Kim et al. (eds.), *Clinical PET and PET/CT: Principles and Applications*,
DOI 10.1007/978-1-4419-0802-5_4, © Springer Science+Business Media New York 2013

infarction [15], and neurologic disease [16, 17]. 2-Deoxy-2-[^{18}F]fluoro-D-glucose was developed in 1976 for the specific purpose of mapping brain glucose metabolism in living humans. After the first synthesis of ^{18}F-FDG via an electrophilic fluorination with ^{18}F gas, small-volume enriched water targets were developed that made it possible to produce large quantities of [^{18}F]fluoride ion via the high yield ^{18}O(p,n)^{18}F reaction. This was followed by a major milestone, the development of a nucleophilic fluorination method that produced [^{18}F]-FDG in very high yields. These advances and the remarkable properties of ^{18}F-FDG have largely overcome the limitations of the 110-min half-life of ^{18}F. Although tumor metabolic imaging using [^{18}F]-FDG has been studied in the past two decades, its clinical application is still hampered by its limitations, such as differentiation of infection and tumor recurrence, and differentiation of low-grade and high-grade tumors [18]. To improve the diagnosis, prognosis, planning, monitoring, and predicting results of the cancer treatment, several other PET imaging agents are used to characterize tumor targets.

Amino Acid Transport

^{11}C-methionine is useful for metabolic imaging of tumors by PET [19]; however, it has too many metabolic pathways that make it difficult to obtain a rate constant [20, 21]. Because of its short half-life, it is also difficult to image tumors with slow uptake. To overcome these drawbacks, L-α-methyltyrosine (L-AmT) has been investigated in nuclear medicine, not only because of its biologic importance in the synthesis of protein or thyroid hormone, but also because of its involvement in dopamine or tyramine neurotransmitters [22]. Its analog, ^{123}I-α-methyltyrosine, has also been used for SPECT studies on brain and pancreatic tumors [23–25]. High accumulation of ^{123}I-α-methyltyrosine (I-LAmT) in tumors were reported. PET examination with ^{124}I-labeled α-methyltyrosine has been carried out in patients with brain tumors [25]. L-^{18}F-α-methyltyrosine (L-^{18}FAmT) was also developed. L-^{18}FAmT was synthesized by reacting L-AmT with $CH_3COO^{18}F$. A similar technique has been used to synthesize ^{18}F-labeled metatyrosine [26]. An electrophilic reactant, $CH_3COO^{18}F$, reacts with L-AmT to give a meta-oriented position on the benzene ring. L-^{18}FAmT is quite stable in vivo compared with 2-^{18}F-fluorotyrosioe [27, 28] or ^{11}C-tyrosine, which produce too many metabolites, thus making it difficult to obtain quantitative analysis [29, 30]. Although the radiochemical yield of L-^{18}FAmT was $20.3 \pm 5.1\%$ ($n = 5$) based on the radioactivity trapped in the reaction vessel, the radiochemistry purification using preparative high-performance liquid chromatography (HPLC) is time consuming. For instance, ^{19}F-nuclear magnetic resonance (NMR) analysis gave two isomer spectra of L-^{19}FAmT with chemical shifts of −57.5 and −61.0 using trifluoroacetic acid as an internal standard [31]. These two isomer product ratios are 1 to 5.6, which corresponds to 2-L-^{19}FAmT and 3-L-^{19}FAmT, respectively. These assignments were based on the isomer of ^{19}F-meta-tyrosine spectra reported by Dejesus et al. [31]. Recently, a rapid synthesis with high yield of O-2-^{18}F-fluoroethyltyrosine was developed [32–34]. Because introducing a methyl group in the α position could slow down the protein incorporation process, ^{18}F-fluoropropyl-AmT (L-^{18}FPAmT) was developed using a similar technique. The synthetic scheme is shown in Fig. 4.1. Both L-^{18}FamT and L-^{18}FPAmT are discussed in this chapter.

Markers of Estrogen Receptor Tissue

The presence of sex hormone receptors in both primary and secondary breast tumors is an important indicator for both prognosis and choice of therapy for the disease [35]. Currently, receptors are determined by in vitro analysis of biopsy specimens and the use of antiestrogens. Tamoxifen is the therapy of choice for estrogen receptor-positive (ER+) tumors. The detection and measurement of ER+ tumors by the use of a radiolabeled ligand should provide a useful tool for the detection of primary and secondary tumors, as it may assist in selecting and following the most favorable therapy, as well as predicting

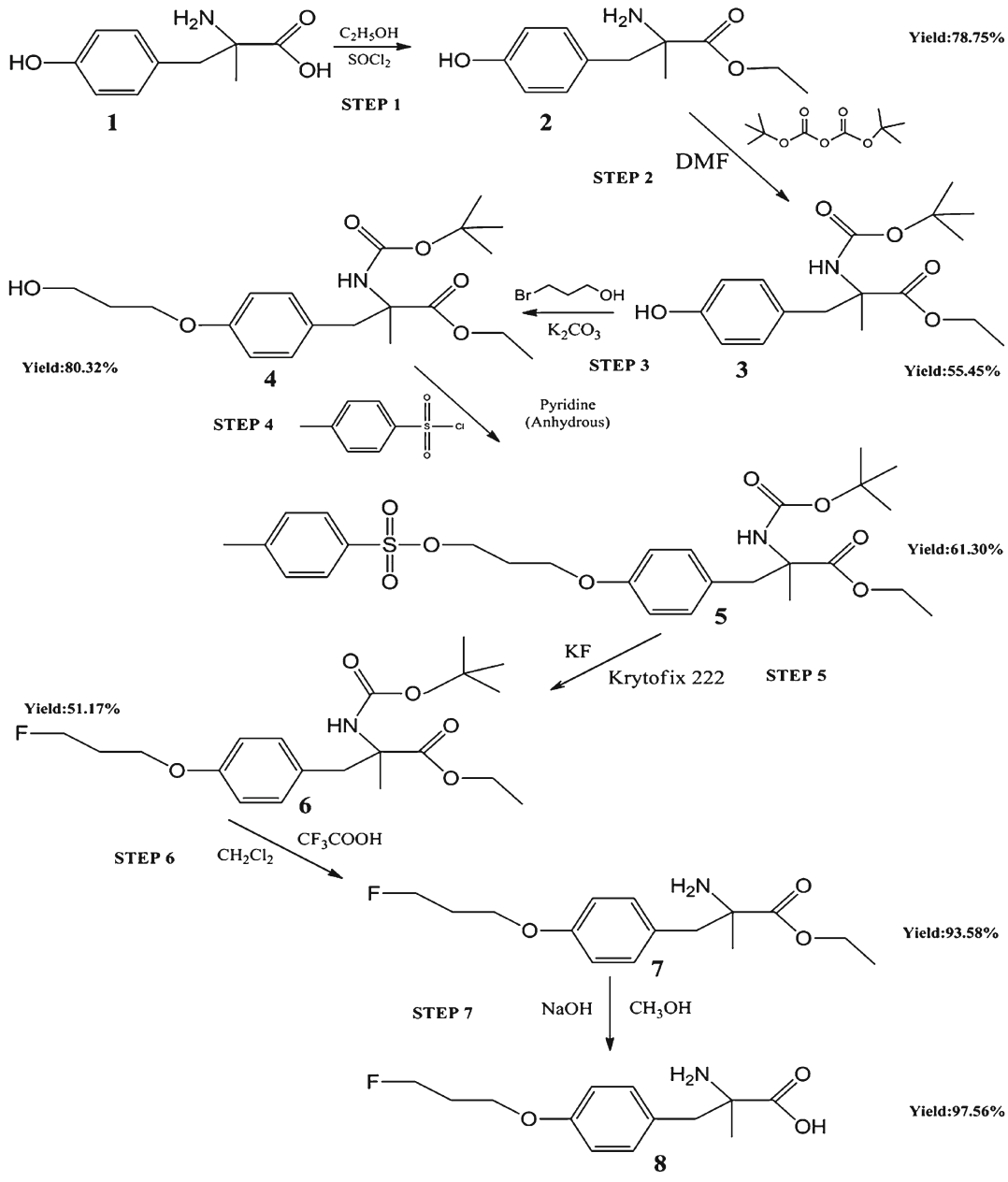

Fig. 4.1 Synthesis of ^{18}F-fluoropropyl-α-methyltyrosine

its outcome. To this end a number of variations of substituted estradiols have been prepared containing the radioisotope fluorine in the 16 position [36–38]. These compounds have been relatively successful in detecting ER-rich tissue in vivo, but their ability to provide quantitative information on receptor concentration in either animal models or humans has been less clearly demonstrated.

Tamoxifen therapy results are positive in 30% of unselected patients with breast cancer. A response rate of 50–60% was obtained in

patients with ER+tumors [39]. Patients with metastatic cancer who do respond to the treatment have a response duration of 10–18 months and prolonged survival [40]. A radiolabeled tamoxifen ligand would be useful in diagnosing diseases that produce high levels of ERs, such as ovarian cancer, endometriosis, uterine carcinoma, and meningioma. Our rationale is that if the binding of the ligands with tumors can be detected with PET or SPECT, then such ligands may predict the response to anticancer agents' therapy for cancer. Radiolabeled tamoxifen would also be useful in investigating tamoxifen's mechanisms of action because it would provide more accurate information about the effectiveness of antiestrogen (tamoxifen) therapy.

Markers of Tumor Hypoxia

Misonidazole (MISO) is a hypoxic cell sensitizer, and labeling MISO with different halogenated radioisotopes (e.g., fluorine-18 or iodine-131) could be useful for differentiating a hypoxic but metabolically active tumor from a well-oxygenated active tumor by PET or planar scintigraphy [41–46]. [^{18}F] Fluoromisonidazole (FMISO) has been used to assess the hypoxic component in brain ischemia, myocardial infarction, and various tumors [47–52]. Moreover, the assessment of tumor hypoxia with labeled MISO prior to radiation therapy would provide a rational means of selecting patients for treatment with radiosensitizing or bioreductive drugs (e.g., mitomycin C). Such selection of patients would permit more accurate evaluation because the use of these modalities could be limited to patients with hypoxic tumors. It is also possible to select proper modalities of radiotherapy (neutron versus photon) by correlating labeled MISO results with tumor response.

It has been reported that MISO produced peripheral sensory neuropathy at the dose level required for radiosensitization [53, 54]. Thus, we have developed new MISO analogs by adding one hydroxymethyl group to MISO. This new ligand (halogenated erythronitroimidazoles; ETNIM) is more hydrophilic than FMISO. We used autoradiograms and radionuclide imaging techniques to demonstrate the potential application of FMISO and fluoro-ETNIM (FETNIM) to diagnose tumor hypoxia.

Markers of Lipid Metabolism

An elevated level of phosphatidylcholine has been found in tumors. It is the most abundant phospholipid in the cell membranes of all eukaryotic cells and provides a potential target for tumor imaging. This elevation is thought to be the result of increased uptake of choline, a precursor of the biosynthesis of phosphatidylcholine. Malignant tumors show a high proliferation and increased metabolism of cell membrane components that will lead to an increased uptake of choline [55]. Thus, [^{11}C]choline can be used as a PET marker for imaging cell membrane proliferation in prostate cancer [56], brain tumors [57], and many other types of tumors [58] that lack the urinary radioactivity seen with ^{18}F-FDG [56, 59]. [^{18}F] Fluorocholine and fluorine-18-labeled choline analogs also have been developed as new and promising oncologic PET tracers for prostate cancer and breast cancer [60–62].

Markers of Tumor Cell Proliferation

Noninvasive imaging assessment of tumor cell proliferation could be helpful in the evaluation of tumor growth potential and the degree of malignancy, and in the early assessment of treatment response prior to changes in tumor size. Radiolabeled nucleoside/nucleotide analogs should provide proliferative imaging information of primary and secondary tumors [28–32]. They may also assist in selecting and following the most favorable choice of nucleoside/nucleotide therapy and in following its outcome. Our rationale is that if the binding of nucleoside/nucleotide to tumor cell DNA/RNA can be detected with PET, then such a nucleoside/nucleotide analog may be useful in evaluating the response of nucleoside/nucleotide (e.g., 5-fluorouracil, 5-fluorodeoxyuridine, 5-bro-

modeoxyuridine, cytidine, cytarabine) therapy for tumors. Thus, for DNA/RNA markers, ^{18}F-fluoroadenosine, ^{18}F-fluorothymidine, and fluoro-^{11}C-methyl-arabinofuranosyluracil were developed. These ligands are intended to improve the understanding of the biologic behavior of malignant tumors, which should lead to better prognostic evaluation, treatment follow-up, and patient management.

Gene Expression Markers

Radiolabeled pyrimidine and purine probes for imaging herpes simplex virus type 1 thymidine kinase (HSV-1-*tk*) expression and other reporter genes by PET have been developed. For example, pyrimidine nucleoside (e.g., FIAU, 2′-fluoro-2′-deoxy-5-iodo-1-β-D-ribo-furanosyl-uracil [FIRU], 2′-fluoro-2′-5-methyl-1-β-D-arabinofuranosyl-uracil [FMAU] 2′-fluoro-2′-deoxy-5-iodovinyl-1-β-D-ribofuranosyl-uracil [IVFRU] and acycloguanosine [9-[(2-hydroxy-1-(hydroxymethyl) ethoxy)methyl]-guanine (GCV) and 9-[4-hydroxy-3-(hydroxymethyl)butyl]guanine (PCV)) [63–68] and other ^{18}F-labeled acycloguanosine analogs, such as 8-fluoro-9-[(2-hydroxy-1-(hydroxymethyl) ethoxy)methyl]guanine (FGCV) [65, 66], 8-fluoro-9-[4-hydroxy-3-(hydroxymethyl)butyl]guanine (FPCV) [67, 68], 9-[3-fluoro-1-hydroxy-2-propoxymethyl]guanine (FHPG) [69, 70], and 9-[4-fluoro-3-(hydroxymethyl)butyl]guanine (FHBG) [71], have been developed as reporter substrates for imaging wild type and mutant [67] HSV-1-*tk* expression. Recently, imaging, pharmacokinetics, and dosimetry of ^{18}F-FHBG were reported in healthy volunteers as a first step to imaging HSV-1-*tk* reporter expression in clinical gene therapy trials [72]. The difficulty with these probes is that HSV-1-*tk* enzyme expression depends on HSV-1-*tk* gene transduction with adenoviral vectors. The level of HSV-1-*tk* enzyme expression is likely to be different in the different transduced cells and tissues; thus, the application of the HSV-1-*tk* probe is limited. Understanding of tumor proliferative activity could aid in the selection of optimal therapy by estimating patient prognosis and selecting the proper management.

Synthetic Materials and Methods for PET Agents

Glucose Transport

A major advance in the synthesis of ^{18}F-FDG from [^{18}F]fluoride was made using kryptofix to increase the reactivity of [^{18}F]fluoride. Kryptofix masks the potassium ions, which are the counter ions of the [^{18}F]fluoride. The reaction of [^{18}F]fluoride with 1,3,4,6-tetra-O-acetyl-2-O-trifluoromethanesulfonyl-B-D-marmopyranase to give 1,3,4,6-tetra-O-acetyl-2-[^{18}F]fluoro-B-D-glycopyranase results in a 95% incorporation of ^{18}F, and the overall synthesis, including purification, proceeds to give approximately a 60% yield. The synthesis involves two steps: displacement with [^{18}F]fluoride and deprotection with HCl.

Amino Acid Transport

A nucleophilic reactant K^{18}F reacts with L-tosylpropyl-AmT to yield ^{18}F-fluoropropyl-AmT (FPAMT, 40–50%). The synthetic scheme is shown in Fig. 4.1.

Markers of Estrogen Receptor Tissue

Using clomiphene, a three-step process to hydroxytamoxifen, tosyl tamoxifen, and halogenated tamoxifen was developed [73, 74]. Eight *cis* and *trans* isomers of halogenated tamoxifen analogs were then prepared. In testing these two conformational isomers, we compared their killing power on human breast tumor cells as well as their binding power. Under our approved investigation of new drugs (IND number 40,589) from the Food and Drug Administration (FDA), we have assessed ER+ breast tumors in 10 patients using ^{18}F-FTX (2–12 mCi IV). In a typical study, a patient is positioned supine in the scanner so that the detector rings span the entire breast. A 20-min attenuation scan is performed with a 4-mCi [68] Ge-ring source prior to administering ^{18}F-FTX. After each patient receives ^{18}F-FTX, six

consecutive 20-min scans are taken. Serial transaxial images are obtained using the scanner (Posicam 6.5, Positron Corp., Houston, TX), which has a field of view of 42 cm on the transverse plane and 12 cm on the coronal plane. The axial resolution in the reconstructed plane is 1.2 cm. Twenty-one transaxial slices separated by 5.2 mm are reconstructed. Visual inspection as well as semiquantitative evaluation using standard uptake value (SUV, the activity in tumor/injected dose × body weight) was used. Before PET scanning, the position of breast tumors is determined by contrast-enhanced CT (High Speed Advantages, General Electric Co., Milwaukee, WI) or MRI using the 1.5-T scanner (GE Medical System, Milwaukee, WI). Eight of ten patients received tamoxifen therapy after the PET study. The response to tamoxifen therapy was evaluated after 6 months.

Markers of Tumor Hypoxia

Synthesis of [^{18}F]FMISO and [^{18}F]FETNIM

Aliquots containing 500–800 mCi of ^{18}F activity after 1-h beam time (18 μA current) were collected. The irradiated water was combined with kryptofix-2,2,2 (26 mg) and anhydrous potassium carbonate (4.6 mg), heated under reduced pressure to remove ^{18}O water, and dried by azeotropic distillation with acetonitrile (3 × 1.5 mL). The tosyl analog of 2-nitroimidazole (20 mg) was dissolved in acetonitrile (1.5 mL), added to the kryptofix-fluoride complex, and then warmed at 95°C for 7 min [42, 52]. After cooling, the reaction mixture was passed through a silica gel Sep-Pak column (Whatman Inc., Clifton, NJ) and eluted with ether (2 × 2.5 mL). The solvent was evaporated and the resulting mixture hydrolyzed with 2 N HCl (1 mL) at 105°C for 7 min. The mixture was cooled under N_2 and neutralized with 2 N NaOH (0.8 mL) and 1 N $NaHCO_3$ (1 mL). The mixture was passed through a short alumina column, a C-18 Sep-Pak column, and a 0.22-μm millipore filter, followed by eluting 6 mL of 10% ethanol/saline. A yield of 80–100 mCi of pure product was isolated (25–40% yield, decay corrected) with the end of bombardment (EOB) at 60 min. HPLC was done on a C-18 ODS-120 T column, 4.6 × 25 mm, with water/acetonitrile, (80/20), using a flow rate of 1 mL/min. The no-carrier-added product corresponded to the retention time (6.12 min) of the unlabeled FMISO under similar conditions. The radiochemical purity was greater than 99%. There were no other impurities under the ultraviolet (UV) ray detector (310 nm). A radio-TLC scanner (Bioscan, Washington, DC) showed a retardation factor of 0.6 for FMISO using a 5 × 20 cm silica gel plate (Whatman, Inc., Clifton, NJ), eluted with chloroform/methanol (7:3), which corresponds to the unlabeled FMISO. In addition, kryptofix-2,2,2 was not visualized (developed in the iodine chamber) on the silica-gel-coated plate using 0.1% (v/v) triethylamine in methanol as art eluent. The specific activity of [^{18}F]FMISO and [^{18}F]FETNIM determined were 1 Ci/μmol based on UV and radioactivity detection of a sample of known mass and radioactivity.

PET Imaging of Head and Neck Tumor Hypoxia Using [18F]FMISO

Under our approved IND number 43,997 from the FDA, we have completed three studies using [^{18}F]FMISO. In a typical study, a patient is positioned supine in the scanner so that the detector rings span the entire head and neck. A 20-min attenuation scan is performed with a 4 mCi [68] Ge-ring source prior to administering [^{18}F]FMISO. After each patient receives 10 mCi of [^{18}F]FMISO, six consecutive 20-min scans are taken. Serial transaxial images are performed using the scanner (Posicam 6.5, Positron Corp., Houston, TX), which has a field of view of 42 cm on the transverse plane and 12 cm on the coronal plane. The axial resolution in the reconstructed plane is 1.2 cm. Twenty-one transaxial slices separated by 5.2 mm are reconstructed and displayed in SUV, which measures the ratio of tissue [^{18}F]FMISO uptake to that of whole-body uptake (normalized for body weight and injected dose) for each scan. Before PET scanning, the position of head and neck tumors is also determined by

contrast-enhanced CT (High Speed Advantages, GE Medical System, Milwaukee, WI).

Autoradiographic Studies of Misonidazole Analogs in Tumor-Bearing Rats

After receiving [^{18}F]FMISO (1–1.5 mCi IV), female Fischer 344 breast tumor-bearing rats and Lewis lung tumor-bearing mice (3/ligand) were euthanized at 1 h. The rodent body was fixed in a carboxymethyl cellulose (4%) block. The frozen body in the block was mounted to a cryostat microtome (LKB, Ijamsville, MD), and 100-ttm coronal sections were made. The section was freeze-dried and then placed on x-ray film (X-Omat AR, Kodak, Rochester, NY) for 24 h.

Polar Graphic Oxygen Needle Probe Measurements

To confirm hypoxic tumors detected by imaging, intratumoral pO_2 measurements were performed using the Eppendorf computed histographic system. Twenty to 25 pO_2 measurements along each of two to three linear tracks were performed at 0.4-mm intervals on each tumor (40–75 measurements total). Tumor pO_2 measurements were made on three tumor-bearing rats and three rabbits. Using an on-line computer system, the pO_2 measurements of each track were expressed as absolute values relative to the location of the measuring point along the track, and as the relative frequencies within a pO_2 histogram between 0 and 100 mmHg with a class width of 2.5 mm.

Markers of Lipid Metabolism

After ^{11}C-carbon dioxide production in a cyclotron and the subsequent ^{11}C-methyl-iodide synthesis, methyl-^{11}C-choline was synthesized by the reaction of ^{11}C-methyl-iodide with "neat" dimethylaminoethanol at 120°C for 5 min. Purification was achieved by evaporation of the reactants followed by passage of the aqueous solution of the product through a cation-exchange resin cartridge. The time required for overall chemical processing, excluding the cyclotron operation, was 15 min. Radiochemical yield was >98%. Radiochemical purity was >98%. Chemical purity was >90% (dimethylaminoethanol was the only possible impurity). Specific radioactivity of the product was >133 GBqb/μmol. PET was performed on cancer patients from the level of the pelvis to the lower abdomen. After transmission scanning, 370 MBq ^{11}C-choline was injected intravenously. The emission scan was performed 5–15 min postinjection. Finally, PET images were displayed so that each pixel was painted by a specified color representing the degree of SUV. The ^{11}C-choline image was compared with the ^{18}F-FDG image obtained from the same patient.

No-carrier-added [^{18}F]fluoroethyl choline [^{18}F]FECh was synthesized by two-step reactions: first, tetrabutylammonium (TBA) ^{18}F-fluoride was reacted with 1,2-bis(tosyloxy)ethane to yield 2-^{18}F-fluoroethyl tosylate; second, 2-^{18}F-fluoroethyl tosylate was reacted with *N,N*-dimethylethanolamine to yield ^{18}F-FECh, which was then purified by chromatography. An automated apparatus was constructed for preparation of the ^{18}F-FECh injection solution. In vitro experiments were performed to examine the uptake of ^{18}F-FECh in Ehrlich ascites tumor cells, and the metabolites were analyzed by solvent extraction followed by various kinds of chromatography. Clinical studies of ^{18}F-FECh PET were performed on patients with untreated primary prostate cancer, and the data were compared with those of ^{11}C-choline PET on the same patients.

Markers of Tumor Cell Proliferation

Using ^{18}F-Fluoro-2′-Deoxyadenosine [9-(2′-Deoxy-2′-Fluoro-b-D-Arabinofuranosyl)Adenine](FAD)

2′-O-p-toluenesulfonyladenosine (100 mg, 0.238 mmol) was derivatized along with N^6, O-3′, and O-5′ acetylated analogs by dissolving in tetrahydrofuran (5 mL) and acetic anhydride (2 mL), along with pyridine (2 mL) [75, 76]. The reaction

was stirred overnight. The solvent, excess of pyridine, and unreacted acetic anhydride were removed by evaporation, and the residue was chromatographed on silica gel (with ethyl acetate as eluent). Aliquots containing 20–40 mCi of [^{18}F]fluoride were combined with kryptofix-2,2,2 and anhydrous potassium carbonate and heated to remove [^{18}O]H_2O. The triacetylated tosyl analog of adenosine was dissolved in acetonitrile, added to the kryptofix-fluoride (fluorine-18) complex, and then heated at 95°C for 10 min. After cooling, the reaction mixture was passed through a silica-gel–packed column (SPE, 500 mg) and eluted with acetonitrile (ACN, 2 mL). After solvent evaporation, the acetyl groups were deprotected with 2 N HCl (1 mL) at 105°C for 10 min. The product was neutralized with 2 N NaOH (0.8 mL) and 1 N $NaHCO_3$ (1 mL). The product was then eluted through a reverse phase C-18 column (Sep-Pak Cartridge, Waters, Milford, MD) and a 0.22-mm filter, followed by saline (3 mL).

Markers of Gene Expression

Using a known procedure, di-tritylated tosylbutylguanine (TsHBG) was synthesized. Mass spectrum and NMR spectrum were determined. Under similar conditions for the synthesis of ^{18}F-fluorinated adenosine, ^{18}F-FHBG was synthesized. A C-18 reverse-phase Sep-Pak was used to purify the compound.

Results of Synthesis for PET Agents

The overall synthesis of ^{18}F-FDG including purification proceeds to result in approximately a 60% yield after displacement with [^{18}F]fluoride and deprotection with HCl. The simplest method to remove kryptofix is the incorporation of a short cation exchange resin in the synthesis system so that the hydrolysate (HCl) passes through the cartridge before final purification; 2-deoxy-2-chloro-D-glucose (CIDG) was identified as an impurity with less than 100 μg during chromatographic determination of the specific activity of ^{18}F-FDG preparations from the nucleophilic route.

Amino Acid Transport

Proton NMR spectrum of L-tosylpropylAmT is shown in Fig. 4.2. Figures 4.3 and 4.4 show HPLC and radio-TLC analysis of [^{18}F]FPAMT. There was a similarity in cellular uptake both in vitro (Fig. 4.5) and in vivo (Fig. 4.6) between [^{18}F]FPAMT and [^{18}F]FDG. Due to a zwitterion, there was much less uptake in brain compared to [^{18}F]FDG. Clinical images indicated that low-grade brain tumor could be imaged with [^{18}F]FPAMT.

Markers of Estrogen Receptor Tissues

Using MCF-7 cells incubated for 72 h, we observed that the eight new compounds were superior in killing power compared with tamoxifen; for example, the bromo had almost 25 times the killing power of tamoxifen [77, 78]. By using pig uterine cytosol, we noted that halogenated tamoxifen had a better binding affinity than tamoxifen itself. Bromotamoxifen was 150 times better than tamoxifen, and fluorotamoxifen had a binding power 30 times that of tamoxifen.

Of these eight different agents, we pursued fluorotamoxifen for its killing and binding power and were interested in using this technology as a PET imaging agent. Using the PET camera, the uterus of a pig was defined. We then administered the fluorotamoxifen and noted a configuration that was much like what we saw in the anatomic specimen, with the uterus and the fallopian-tube–ovarian complex. From the cross-sectional configuration it appears that fluorotamoxifen can be used as an imaging agent as well. By administering tamoxifen, or diethylstilbestrol (DES), the uptake in the target organ could be blocked [79]. As a breast tumor model, we used a rat with deposition of ER+tumor cells (NF 13762 cell line) in the flank. In utilizing fluorotamoxifen, we observed uptake within the uterus as well as in the tumor in the flank, which suggests we have a fluorinated

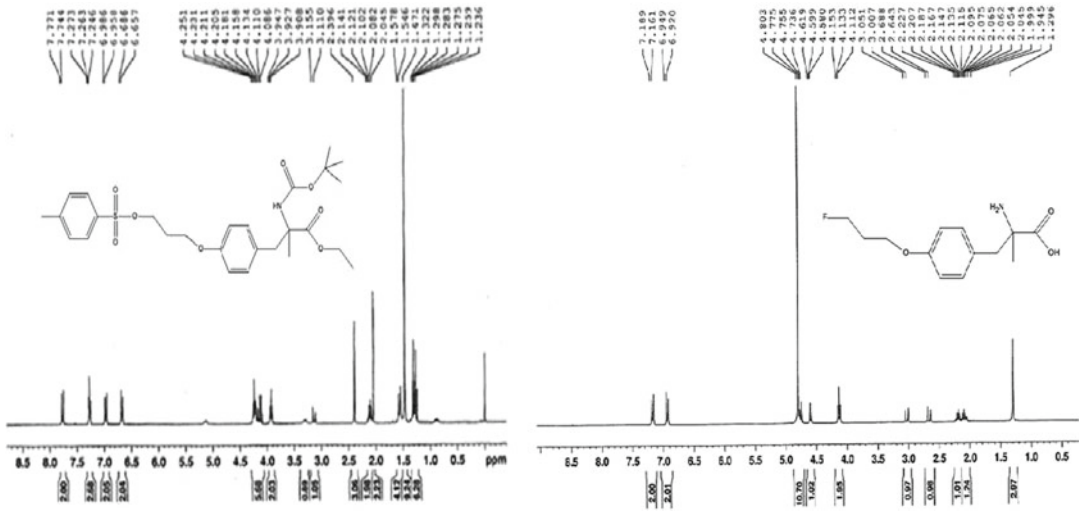

Fig. 4.2 ^{1}H-NMR of N-BOC-tosylpropyl-α-methyltyrosine methyl ester

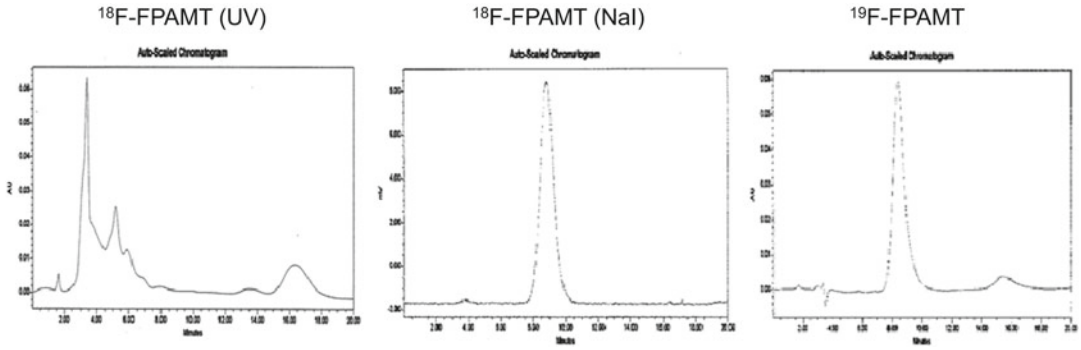

Fig. 4.3 High-performance liquid chromatography (HPLC) analysis of ^{18}F-FPAMT (*left*: radioactive, *right*: ultraviolet [UV])

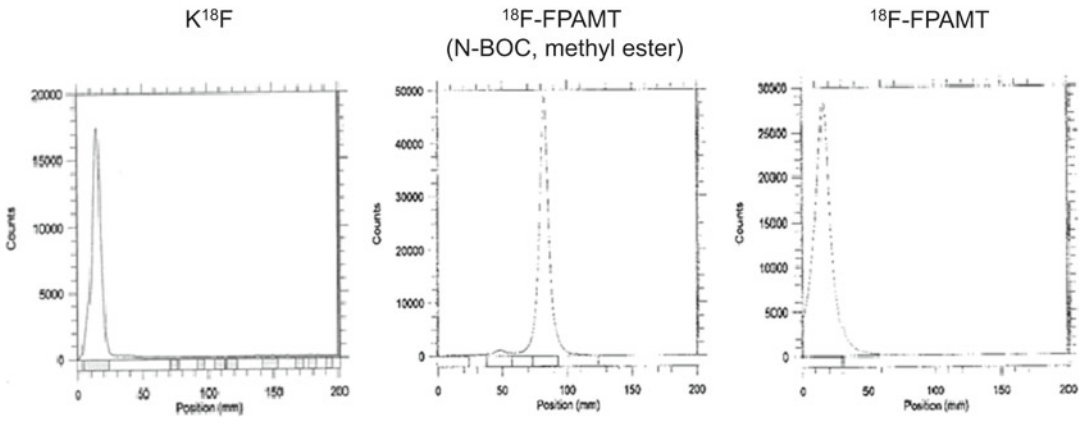

Fig. 4.4 Radio-TLC analysis of ^{18}F-FPAMT

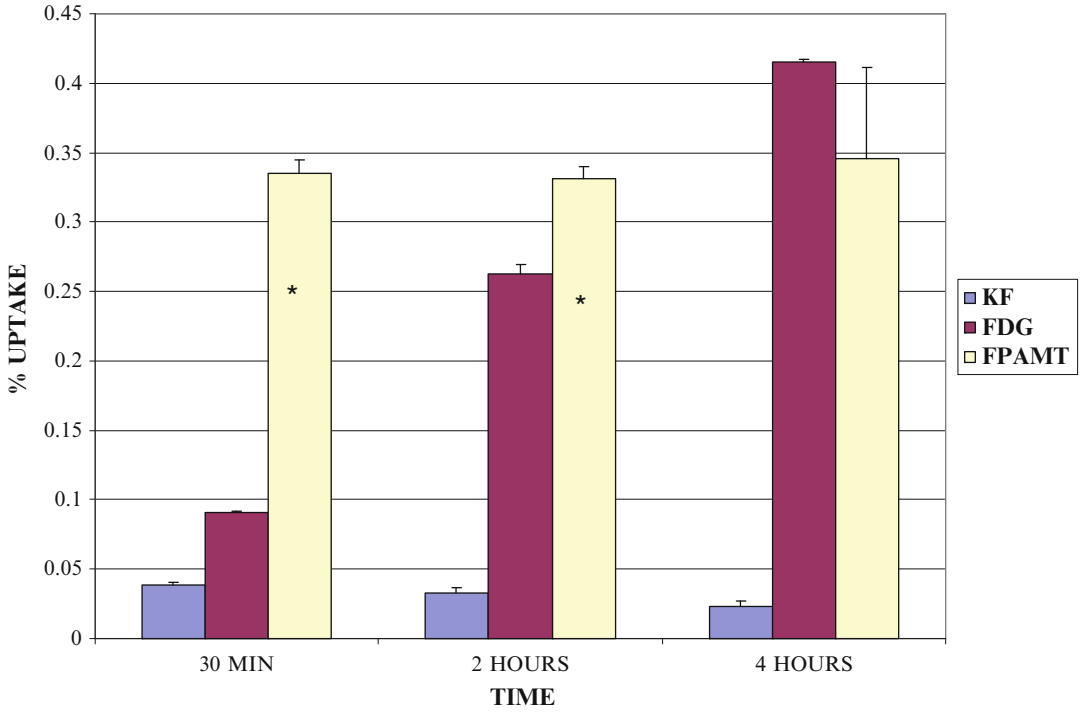

Fig. 4.5 Cellular uptake of ^{18}F-FDG and ^{18}F-FPAMT in breast cancer cell line

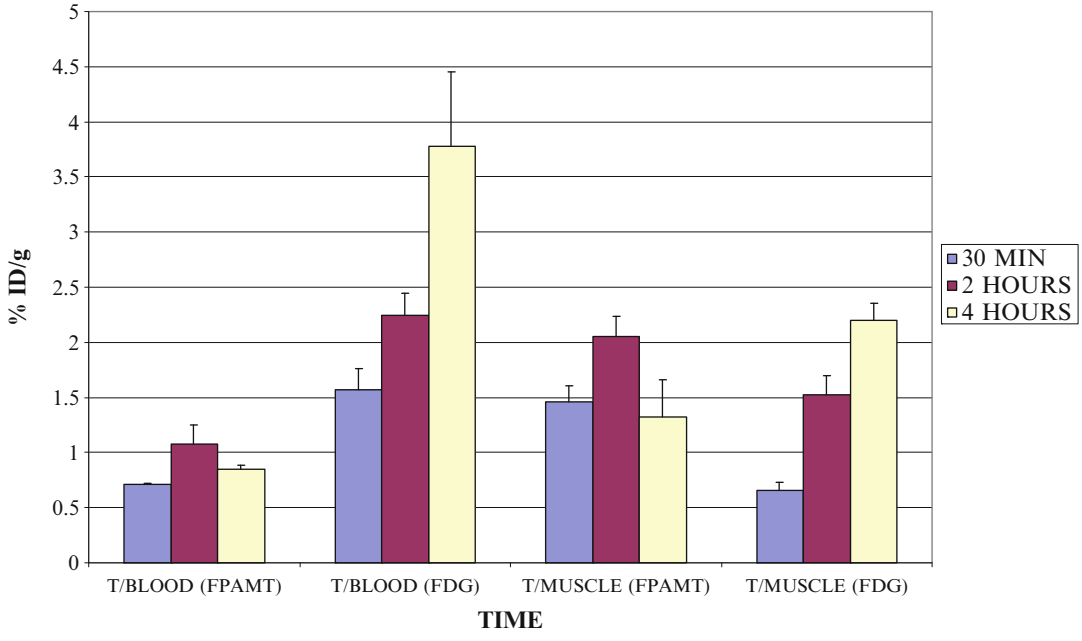

Fig. 4.6 Tumor-to-tissue count density ratios of ^{18}F-FDG and ^{18}F-FPAMT in breast tumor-bearing rats

Table 4.1 PET results of diagnostic accuracy

	Sensitivity	Specificity
C-11 choline	67% (18/27 lesions)	95% (53/56 lesions)
FDG	48% (13/27 lesions)	100% (56/56 lesions)

tamoxifen that can readily visualize ER sites, even in the implanted neoplasm. In studying the distribution, we noted fairly good uptake in the tumor, brain, and liver. We found fairly good biodistribution in the uterus/blood count ratio. The count ratio was 13.5, and the uterine uptake could be blocked somewhat by any of the estrogens or by tamoxifen itself. Fluorotamoxifen can be prepared as an analog of tamoxifen itself with high specific activity, and it can image ER+ sites in the animal models and in humans [80, 81]. In addition, such ligands might help in determining the causes of occasional failure of tamoxifen therapy when biopsy indicators are ER+.

To date we have used an ^{18}F-labeled tamoxifen ligand (2–12 mCi IV) to image 10 patients with ER+ breast tumors (IND number 40,589) by PET. We found that it is possible to visualize both primary and metastatic breast tumors by their uptake of the radiolabeled tamoxifen ligand. Of the ten patients, three had tumors that showed good uptake of the radiolabeled ligand and positive responses to tamoxifen therapy [82, 83]. However, we observed high uptake in the liver and lung, which affected the imaging and created difficulty in interpretation of tumors near those organs. Others have also reported that liver and lung tamoxifen uptake levels can remain high between 3 and 14 days of therapy.

Markers of Tumor Hypoxia

Autoradiographs of ^{18}F-FMISO showed that tumor necrotic region could be differentiated. Clinical PET studies showed that the tumors could be well visualized on ^{18}F-FMISO and ^{18}F-FETNIM tests. The tumor oxygen tension was 3–6 mm Hg as compared with the normal, 30–40 mm Hg.

Marker of Lipid Metabolism

Imaging of prostate cancer and its local metastasis was difficult when ^{18}F-FDG was used because within the pelvis, the areas of high uptake were concealed by the overwhelmingly abundant radioactivity in urine (in ureters and bladder). By contrast, it was easy when ^{11}C-choline was used because the urinary activity was negligible and tumor uptake was marked. The radioactivity concentration of ^{11}C-choline in prostate cancer and metastatic sites was at an SUV of more than 3 in most cases. The SUV of ^{18}F-FDG was considerably lower than that of ^{11}C-choline. The sensitivity and specificity of ^{18}F-FDG and ^{11}C-choline are shown in Table 4.1. ^{18}F-FECh was prepared in high yield and purity. The in vitro experiment revealed that ^{18}F-FECh was incorporated into tumor cells by active transport, then phosphorylated (yielding phosphoryl^{18}F-FECh) in the cells, and finally integrated into phospholipids. The clinical PET studies showed marked uptake of ^{18}F-FECh in prostate cancer [60, 61]. A dynamic PET study on one patient revealed that the blood level of ^{18}F-FECh decreased rapidly (in 1 min), the prostate cancer level became almost maximal in a short period (1.5 min) and remained constant for a long period of time (60 min), and the urinary radioactivity became prominent after a short time lag (5 min). Static PET studies conducted under bladder irrigation showed no difference between ^{18}F-FECh uptake and ^{11}C-choline uptake in prostate cancer. However, ^{18}F-FECh gave a slightly higher spatial resolution of the image, which was attributed to the shorter positron range of ^{18}F. The synthesis of ^{18}F-FECh was easy and reliable. ^{18}F-FECh PET was very effective in detecting prostate cancer in patients.

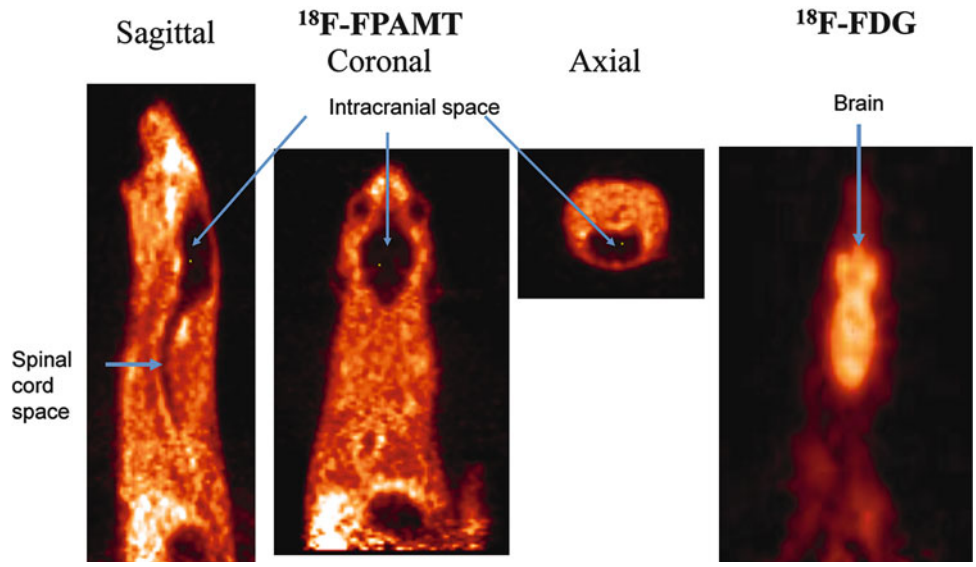

Fig. 4.7 Structure of ^{18}F-fluorinated adenosine

Fig. 4.8 Structure of ^{18}F-fluorinated fluoroethyl uracil

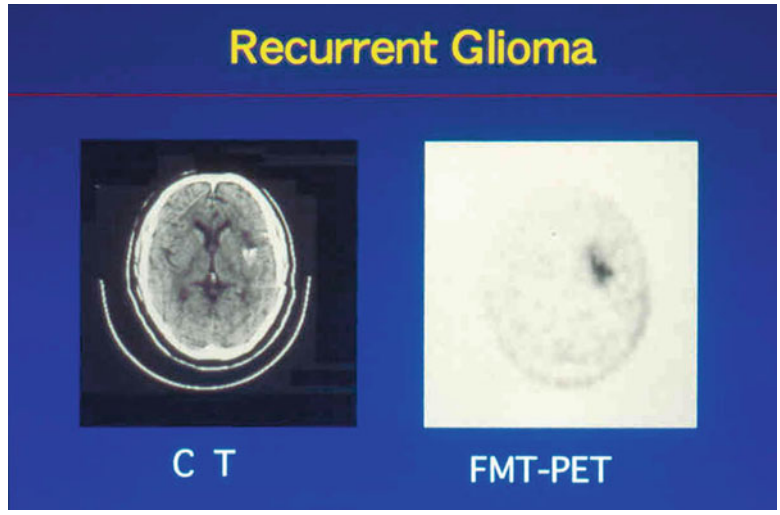

Markers of Tumor Cell Proliferation

The radioactivity of the final product (structure shown in Fig. 4.7 was 7–15 mCi, 50–60%, decay corrected) with the end of bombardment at 70 min. Under similar condition, ^{18}F-fluorinated uracil (structure shown in Fig. 4.8) was synthesized. An autoradiogram showed that the tumor could be visualized with ^{18}F-fluorinated uracil.

Markers of Gene Expression

Using a known procedure, di-tritylated tosylpenclovir (TsHBG) was synthesized. Mass spectrum and NMR spectrum are shown in Figures 4.9 and 4.10. Under similar condition for the synthesis of ^{18}F-fluorinated adenosine, ^{18}F-FHBG was synthesized. A C-18 reverse phase Sep-Pak was used to purify the compound. The radiochemical yield of

Fig. 4.9 Mass spectrometry of di-tritylated tosylpenciclovir

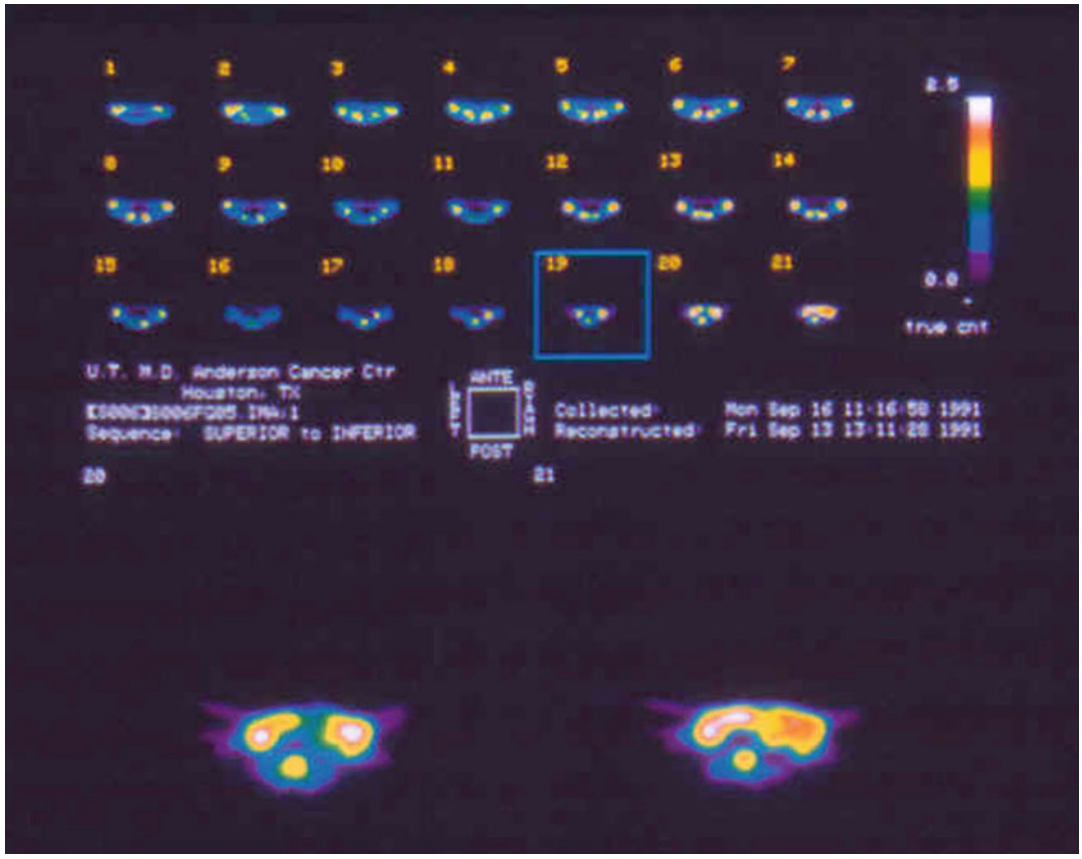

Fig. 4.10 ^{19}F-nuclear magnetic resonance of tosyl chloride and di-tritylated tosylpenciclovir

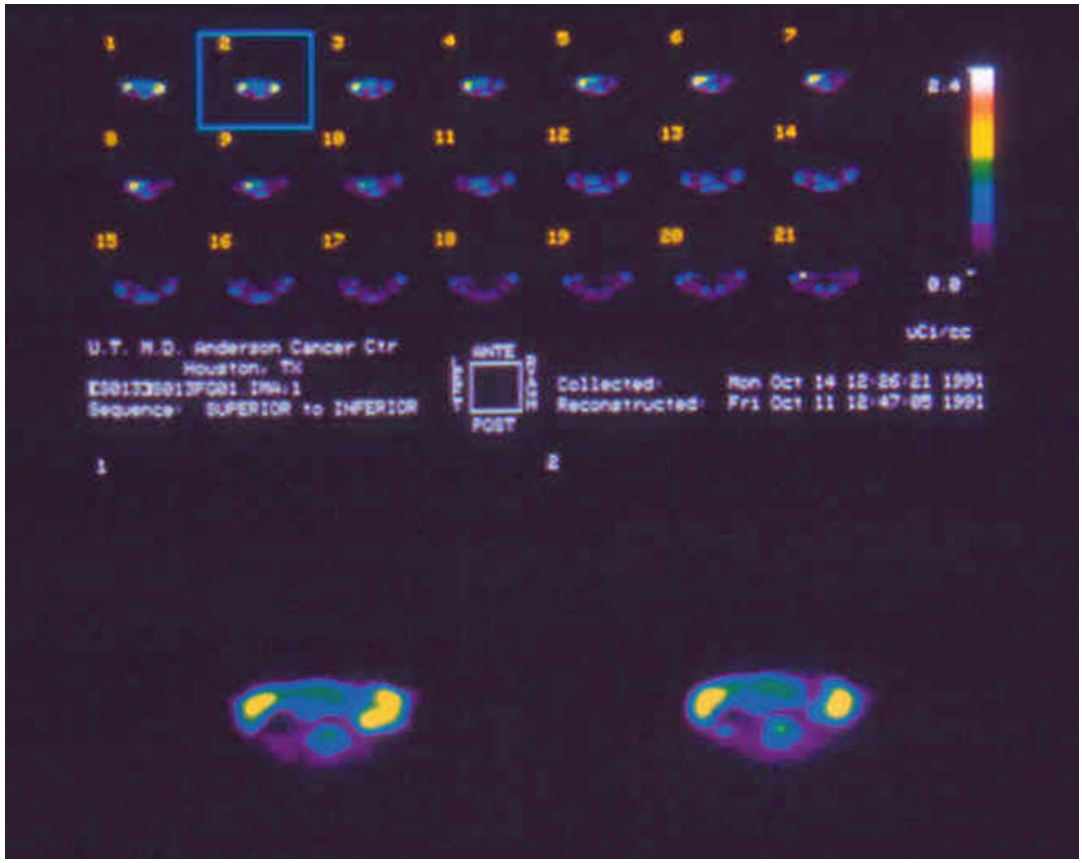

Fig. 4.11 Radiosynthesis of ^{18}F-FHBG

^{18}F-FHBG was 10–15% (decay corrected), with the end of bombardment at 90 min. Radio-TLC is shown in Fig. 4.11.

Discussion

Placing an iodine atom or a fluorine atom on the aromatic ring of tamoxifen has been previously reported [84, 85]. These analogs produced either low affinities for estrogen receptors or low specific activities, neither suitable for imaging estrogen responsive tissues. When ^{11}C-labeled tamoxifen was synthesized, the specific activity was also low [86]. Placing a chlorine atom on the aliphatic side chain of tamoxifen produced a higher affinity than that of tamoxifen [87]. However, this compound is not suitable for imaging purposes because there is no existing cyclotron-produced isotope for chlorine. Previous studies by our group indicate that replacing a chlorine with a halomethyl group develops a higher binding affinity for tamoxifen.

At present, 10 patients with ER+ breast tumors (IND number 40,589) using ^{18}F-labeled tamoxifen ligand (2–12 mCi IV) were imaged by PET. Both primary and metastatic breast tumors could be diagnosed by ^{18}F-labeled tamoxifen ligands. Three lesions in three patients were considered to be truly negative for breast cancer

on the basis of biopsy specimens and/or clinical course. Five of seven patients (71.4%) and 16 of 20 lesions (80%) were interpreted to be truly positive for breast cancer. The mean SUV of the radiotracer in tumor was 2.8 on delayed images. There was no significant correlation between the SUV of [^{18}F]fluorotamoxifen in the lesion and the ER concentration in primary or metastatic lesions. Eight of ten patients received tamoxifen therapy after the PET study. Three patients who had a good response to tamoxifen therapy showed an SUV of [^{18}F]fluorotamoxifen of more than 2.4 in the tumor, whereas four of five patients who had a poor response to tamoxifen therapy showed an SUV of [^{18}F]fluorotamoxifen of less than 2.0 in the lesion. PET imaging using [^{18}F]fluorotamoxifen as the radiotracer provides useful information in predicting the effect of tamoxifen therapy in patients with recurrent or metastatic ER+ breast cancer. Results from the present study also indicate that radioiodinated and indium-labeled tamoxifen analogs are feasible to diagnose ER+ lesions.

The key to the development of ^{18}F-FMISO is to prepare (2′-nitro-1′-imidazolyl)-2-O-acetyl-3-O-tosylpropanol precursor. This intermediate could be prepared easily by treatment of 2-acetyl-1,3-ditosyl glycerol and 2-nitroimidazole as described previously. Both labeled compounds produced sufficient radioactivity and high radiochemical purity. Others have used ^{18}F-epifluorohydrin with 2-nitroimidazole or 1,3-ditosyl-O-tetrahydropyran to react with 2-nitroimidazole, followed by ^{18}F-displacement. These reactions take longer synthetic steps, have a longer reaction time, or provide lower radiochemical yield. Numerous in vitro and in vivo experiments have shown that cells irradiated under low oxygen tensions are more resistant to the lethal effects of low linear energy transfer (LET) ionized radiation compared with cells irradiated under “normal” oxygen tensions. Our clinical trial with PET demonstrated that ^{18}F-FMISO is capable of providing functional images of tumor hypoxia. Autoradiographs of all four analogs showed that tumor hypoxia could be easily demonstrated in rodents. Tumor oxygen tension was determined to be 3.2–6.0 mm Hg, whereas normal muscle tissue had 30–40 mm Hg.

Because tumor uptake of ^{11}C-choline is higher than that of ^{18}F-FDG (i.e., synovial sarcoma), and shorter imaging time is required for ^{11}C-choline, ^{11}C-choline appeared to be a promising PET tracer. There was no effect on tumor uptake in patients with diabetes mellitus. ^{11}C-choline is feasible for detecting intrapelvic lesions because of low urinary excretion. ^{18}F-fluorinated choline revealed in vitro phosphorylation was similar to that of choline. The PET images of a patient with recurrent prostate cancer showed uptake of ^{18}F-fluorinated choline in the prostatic bed and in metastases to lymph nodes. ^{18}F-fluorinated choline PET showed uptake in malignancies in a patient with metastatic breast cancer. PET revealed ^{18}F-fluorinated choline uptake in biopsy-proven recurrent brain tumor with little confounding uptake by normal brain tissues. The ^{18}F-fluorinated choline may serve as a probe of choline uptake and phosphorylation in cancer cells. Preliminary PET studies on patients with prostate cancer, breast cancer, or brain tumor support further studies to evaluate the usefulness of fluorocholin (FCH) as an oncologic probe.

To enhance the biologic activity and increase chemical or metabolic stability, fluorine substitution at the C2′ position of the sugar moiety (arabino configuration) has been widely investigated in drug research [88–90]. [^{18}F]FAD is structurally closer to 2′-deoxyadenosine due to the similarity in the van der Waals radii between the C-H bond and C-halogen bond. Deep-seated tumors in blood-rich organs may require significantly higher ratios for assessment of proliferation. Tumor-to-muscle ratios of [^{18}F]FAD at 2 and 4 h postinjection were 5.2 and 14.3, respectively. Tumor-to-blood ratios at the same time intervals were 2.8 and 5.3, respectively. These data were considered to be acceptable as a tumor imaging agent. Although many other radiopharmaceuticals could be used for assessment of tumor proliferation or metabolic activity, the choice should be determined not only by the biologic behavior of radiopharmaceuticals, but also by their ease of

preparation, as well as by the logistics of imaging.

Although we have synthesized FHBG, we have not conducted preclinical studies. Results from other studies showed that FHBG is a promising PET gene expression probe. For instance, Inubushi et al. [91] showed that HSV-1-*sr*39*tk* reporter gene expression can be monitored with ^{18}F-FHBG and micro-PET in rat myocardium quantitatively and serially with high detection sensitivity. Cardiac PET reporter gene imaging offers the potential of monitoring the expression of therapeutic genes in cardiac gene therapy. Tjuvajev et al. [92] also concluded that the in vitro and in vivo results (including the PET images) show that FIAU is a substantially more efficient probe than FHBG or FHPG for imaging HSV1-*tk* expression, with greater sensitivity and contrast as well as lower levels of abdominal background radioactivity at 2 and 24 h. Alauddin et al. [71] concluded that ^{18}F-FHBG may yield high-contrast PET images of HSV-*tk* expression in tumors. Thus, it is a very promising radiotracer for monitoring of gene therapy of cancer with PET.

Acknowledgments The animal research reported here is supported by a Cancer Center Core grant, NIH-NCI CA-16672.

References

1. Bar-Shalom R, Valdivia AY, Blaufox MD. PET imaging in oncology. Semin Nucl Med. 2000;30:150–85.
2. Plowman PN, Saunders CA, Maisey M. On the usefulness of brain PET scanning to the paediatric neuro-oncologist. Br J Neurosurg. 1997;11:525–32.
3. Weber WA, Avril N, Schwaiger M. Relevance of positron emission tomography (PET) in oncology. Strahlenther Onkol. 1999;175:356.
4. Lau CL, Harpole DH, Patz E. Staging techniques for lung cancer. Chest Surg Clin North Am. 2000;10(4):781–801.
5. Schulte M, Brecht-Krauss D, Heymer B, et al. Grading of tumors and tumor like lesions of bone: evaluation by FDG PET. J Nucl Med. 2000;41(10):1695–701.
6. Yutani K, Shiba E, Kusuoka H, et al. Comparison of FDG-PET with MIBI-SPECT in the detection of breast cancer and axillary lymph node metastasis. J Comput Assist Tomogr. 2000;24(2):274–80.
7. Franzius C, Sciuk J, Daldrup-Link HE, et al. FDG-PET for detection of osseous metastases from malignant primary bone tumors: comparison with bone scintigraphy. Eur J Nucl Med. 2000;27(9):1305–11.
8. Folpe AL, Lyles RH, Sprouse JT, et al. (F-18) fluorodeoxyglucose positron emission tomography as a predictor of pathologic grade and other prognostic variables in bone and soft tissue sarcoma. Clin Cancer Res. 2000;6(4):1279–87.
9. Meyer PT, Spetzger U, Mueller HD, et al. High F-18 FDG uptake in a low-grade supratentorial ganglioma: a positron emission tomography case report. Clin Nucl Med. 2000;25(9):694–7.
10. Franzius C, Sciuk J, Brinkschmidt C, et al. Evaluation of chemotherapy response in primary bone tumors with F-18 FDG positron emission tomography compared with histologically assessed tumor necrosis. Clin Nucl Med. 2000;25(11):874–81.
11. Carretta A, Landoni C, Melloni G, et al. 18-FDG positron emission tomography in the evaluation of malignant pleural diseases – a pilot study. Eur J Cardiothorac Surg. 2000;17(4):377–83.
12. Torre W, Garcia-Velloso MJ, Galbis J, et al. FDG-PET detection of primary lung cancer in a patient with an isolated cerebral metastasis. J Cardiovasc Surg. 2000;41(3):503–5.
13. Brunelle F. Noninvasive diagnosis of brain tumors in children. Childs Nerv Syst. 2000;16(10–11):731–4.
14. Mankoff DA, Dehdashti F, Shields AF. Characterizing tumors using metabolic imaging: PET imaging of cellular proliferation and steroid receptors. Neoplasia. 2000;2:71.
15. Fitzgerald J, Parker JA, Danias PG. F-18 fluorodeoxyglucose SPECT for assessment of myocardial viability. J Nucl Cardiol. 2000;7(4):382–7.
16. Schwarz A, Kuwert T. Nuclear medicine diagnosis in diseases of the central nervous system. Radiology. 2000;40(10):858–62.
17. Roelcke U, Leenders KL. PET in neuro-oncology. J Cancer Res Clin Oncol. 2001;127(1):2–8.
18. Brock CS, Meikle SR, Price P. Does ^{18}F-fluorodeoxyglucose metabolic imaging of tumors benefit oncology? Eur J Nucl Med. 1997;24:691–705.
19. Syrota A, Comar D, Cerf M, et al. [^{11}]C-methionine pancreatic scanning with positron emission computed tomography. J Nucl Med. 1979;20:778–81.
20. Syrota A, Duquesnoy N, Dasaf A, et al. The role of positron emission tomography in the detection of pancreatic disease. Radiology. 1982;143:249–53.
21. Kubota K, Yamada K, Fukuda H, et al. Tumor detection with carbon-11 labeled amino acid. Eur J Nucl Med. 1984;9:136–40.
22. Hagenfeldt L, Venizelos N, Bjerkenstedt L, et al. Decreased tyrosine transport in fibroblasts from schizophrenic patients. Life Sci. 1987;41:2749–57.
23. Tisljar U, Kloster G, Stocklin G. Accumulation of radioiodinated L-alpha-methyltyrosine in pancreas of mice: concise communication. J Nucl Med. 1979;20:973–6.
24. Kloss G, Leven M. Accumulation of radioiodinated tyrosine derivatives in the adrenal medulla and in melanomas. Eur J Nucl Med. 1979;4:179–86.
25. Langen KJ, Coenen HH, Roosen N, et al. SPECT studies of brain tumors with L-3-[^{123}I]-Iodo-alpha-methyl tyrosine: comparison with PET, ^{124}IMT and first clinical results. J Nucl Med. 1990;31:281–6.

26. Tomiyoshi K, Hirano T, Inoue T, et al. Positron emission tomography for evaluation of dopaminergic function using a neurotransmitter analog L-^{18}F-m-tyrosine in monkey brain. Bioimages. 1996;4(1):1–7.
27. Wienhard K, Herholz K, Coenen HH, et al. Increased amino acid transport into brain tumors measured by PET of L-(2-^{18}F)fluorotyrosine. J Nucl Med. 1991; 32:1338–46.
28. Coenen HH, Kling P, Stocklin G, et al. Metabolism of L2-^{18}F-fluorotyrosine, new PET tracer for protein synthesis. J Nucl Med. 1989;301:367–1372.
29. Ishiwata K, Valvurg W, Elsigna PH, et al. Metabolic studies with L-^{11}C-tyrosine for the investigation of a kinetic model of measuring protein synthesis rate with PET. J Nucl Med. 1988;29:524–9.
30. Bolster JM, Valburg W, Paans AMJ, et al. Carbon-11 labeled tyrosine to study tumor metabolism by positron emission tomography (PET). Eur J Nucl Med. 1986;12:321–4.
31. Dejesus OT, Sunderland JJ, Nicles R, et al. Synthesis of radiofluorinated analogs of m-tyrosine as potential L-dopatracers via direct reaction with acetylhypofluorite. Appl Radiat Isot. 1990;41(5):433–7.
32. Tang G, Wang M, Tang X, et al. Pharmacokinetics and radiation dosimetry estimation of O-(2-[18 F]fluoroethyl)-L-tyrosine as oncologic PET tracer. Appl Radiat Isot. 2003;58(2):219–25.
33. Hamacher K, Coenen HH. Efficient routine production of the ^{18}F-labelled amino acid O-2-^{18}F fluoroethyl-L-tyrosine. Appl Radiat Isot. 2002;57(6):853–6.
34. Rau FC, Weber WA, Wester HJ, et al. O-(2-[(18)F] Fluoroethyl)-L-tyrosine (FET): a tracer for differentiation of tumour from inflammation in murine lymph nodes. Eur J Nucl Med Mol Imaging. 2002;29(8): 1039–46.
35. Fernandez MD, Burn JI, Sauven PD, et al. Activated estrogen receptors in breast cancer and response to endocrine therapy. Eur J Cancer Clin Oncol. 1984;20:41–6.
36. McGuire AH, Dehdashti F, Siegel BA, et al. Positron tomographic assessment of 16-alpha-[^{18}F]fluoro-17-beta-estradiol uptake in metastatic breast carcinoma. J Nucl Med. 1991;32:1526–31.
37. McManaway ME, Jagoda EM, Kasid A, et al. [^{125}I]17-beta-iodovinyl-11-beta-methoxyestradiol: interaction in vivo with ERS in hormone independent MCF-7 human breast cancer transfected with V-ras H oncogene. Cancer Res. 1987;47:2945–8.
38. Jagoda EM, Gibson RE, Goodgold H, et al. [^{125}I]17-Iodovinyl-11-beta-methoxyestradiol: in vivo and in vitro properties of a high affinity estrogen-receptor radiopharmaceutical. J Nucl Med. 1984;25:472–7.
39. Hamm JT, Allegra JC. Hormonal therapy for cancer. In: Witts RE, editor. Manual of oncologic therapeutics. New York: Lippincott; 1991. p. 122–6.
40. Wittliff JL. Steroid-hormone receptor in breast cancer. Cancer Res. 1984;53:630–43.
41. Rasey JS, Nelson NJ, Chin L, et al. Characterization of the binding of labeled fluoromisonidazole in cells in vitro. Radiat Res. 1990;122:301–8.
42. Cherif A, Yang DJ, Tansey W, et al. Synthesis of [^{18}F]fluoromisonidazole. Pharm Res. 1994;11:466–9.
43. Hwang DR, Dence CS, Bonasera TA, et al. No-carrier-added synthesis of 3-[^{18}F]fluoro-1-(2-nitro-1-imidazolyl)-2-propanol. A potential PET agent for detecting hypoxic but viable tissues. Int J Radiat Appl Instrum A. 1989;40:117–26.
44. Jerabeck PA, Patrick TB, Kilbourn D, et al. Synthesis and biodistribution of ^{18}F-labeled fluoronitroimidazoles: potential in vivo markers of hypoxic tissue. Appl Radiat Isot. 1986;37:599–605.
45. Parliament MB, Chapman JD, Urtasun RC, et al. Noninvasive assessment of tumor hypoxia with ^{123}I-iodoazomycin arabinoside: preliminary report of a clinical study. Br J Cancer. 1992;65:90–5.
46. Valk PET, Mathis CA, Prados MD, et al. Hypoxia in human gliomas: demonstration by PET with [^{18}F]fluoromisonidazole. J Nucl Med. 1992;33:2133–7.
47. Martin GV, Caldwell JH, Rasey JS, et al. Enhanced binding of the hypoxic cell marker [^{18}F]fluoromisonidazole in ischemic myocardium. Nucl Med. 1989;30:194–201.
48. Martin GV, Cardwell JH, Graham MM, et al. Nonivasive detection of hypoxic myocardium using [^{18}F]fluoromisonidazole and PET. J Nucl Med. 1992;33:2202–8.
49. Yeh SH, Liu RS, Hu HH, et al. Ischemic penumbra in acute stroke: demonstration by PET with fluorine-18 fluoromisonidazole. J Nucl Med. 1994;35(5):205. abst.
50. Yeh SH, Liu RS, Wu LC, et al. Fluorine-18 fluoromisonidazole tumour to muscle retention ratio for the detection of hypoxia in nasopharyngeal carcinoma. Eur J Nucl Med. 1996;23(10):1378–83.
51. Liu RS, Yeh SH, Chang CP, et al. Detection of odontogenic infections by [F-18]fluoromisonidazole. J Nucl Med. 1994;35(5):113. abst.
52. Yang DJ, Wallace S, Cherif A, et al. Development of F-18-labeled fluoroerythronitroimidazole as a PET agent for imaging tumor hypoxia. Radiology. 1995;194:795–800.
53. Cherif A, Wallace S, Yang DJ, et al. Development of new markers for hypoxic cells: [^{131}I]iodomisonidazole and [^{131}I]iodoerythronitroimidazole. J Drug Target. 1996;4(1):31–9.
54. Inoue T, Yang DJ, Wallace S, et al. Evaluation of [^{131}I] iodoerythronitroimidazole as a predictor for the radiosensitizing effect. Anticancer Drugs. 1996;7(8): 858–65.
55. Podo F. Tumor phospholipid metabolism. NMR Biomed. 1999;12:413–39.
56. Hara T, Kosaka N, Kishi H. PET imaging of prostate cancer using carbon-11-choline. J Nucl Med. 1998; 39:990–5.
57. Hara T, Kosaka N, Shinoura N, et al. PET imaging of brain tumor with [methyl-^{11}C]choline. J Nucl Med. 1997;38:842–7.
58. Hara T, Kosaka N, Kishi H, et al. Imaging of brain tumor, lung cancer, esophagus cancer, colon cancer, prostate cancer, and bladder cancer with [C-11]choline. J Nucl Med. 1997;38:250P.

59. Kotzerke J, Prang J, Neumaier B, et al. Experience with carbon-11 choline positron emission tomography in prostate carcinoma. Eur J Nucl Med. 2000;27:1415–9.
60. DeGrado TR, Baldwin SW, Wang S, et al. Synthesis and evaluation of (18)F-labeled choline analogs as oncologic PET tracers. J Nucl Med. 2001;42(12): 1805–14.
61. Price DT, Coleman RE, Liao RP, et al. Comparison of [^{18}F]fluorocholine and [^{18}F]fluorodeoxyglucose for positron emission tomography of androgen dependent and androgen independent prostate cancer. J Urol. 2002;168(1):273–80.
62. DeGrado TR, Reiman RE, Price DT, et al. Pharmacokinetics and radiation dosimetry of 18 F-fluorocholine. J Nucl Med. 2002;43(1):92–6.
63. Haberkorn U, Khazaie K, Morr I, et al. Ganciclovir uptake in human mammary carcinoma cells expressing herpes simplex virus thymidine kinase. Nucl Med Biol. 1998;25:367–73.
64. Gambhir SS, Barrio JR, Wu L, et al. Imaging of adenoviral-directed herpes simplex virus type 1 thymidine kinase reporter gene expression in mice with radiolabeled ganciclovir. J Nucl Med. 1998;39: 2003–11.
65. Gambhir SS, Barrio JR, Phelps ME, et al. Imaging adenoviral-directed reporter gene expression in living animals with positron emission tomography. Proc Natl Acad Sci USA. 1999;96:2333–8.
66. Namavari M, Barrio JR, Toyokuni T, et al. Synthesis of 8-[^{18}F]fluoroguanine derivatives: in vivo probes for imaging gene expression with positron emission tomography. Nucl Med Biol. 2000;27:157–62.
67. Gambhir SS, Bauer E, Black ME, et al. A mutant herpes simplex virus type 1 thymidine kinase reporter gene shows improved sensitivity for imaging reporter gene expression with positron emission tomography. Proc Natl Acad Sci USA. 2000;97:2785–90.
68. Iyer M, Barrio JR, Namavari M, et al. 8-[^{18}F] Fluoropenciclovir: an improved reporter probe for imaging HSV1-tk reporter gene expression in vivo using PET. J Nucl Med. 2001;42:96–105.
69. Alauddin MM, Conti PS, Mazza SM, et al. 9-[(3-[^{18}F]-Fluoro-1-hydroxy-2-propoxy)methyl]guanine ([^{18}F]-FHPG): a potential imaging agent of viral infection and gene therapy using PET. Nucl Med Biol. 1996;23:787–92.
70. Alauddin MM, Shahinian A, Kundu RK, et al. Evaluation of 9-[(3-^{18}F- fluoro-1-hydroxy-2-propoxy) methyl]guanine ([^{18}F]-FHPG) in vitro and in vivo as a probe for PET imaging of gene incorporation and expression in tumors. Nucl Med Biol. 1999;26:371–6.
71. Alauddin MM, Conti PS. Synthesis and preliminary evaluation of 9-(4-[^{18}F]-fluoro-3-hydroxymethylbutyl) guanine ([^{18}F]FHBG): a new potential imaging agent for viral infection and gene therapy using PET. Nucl Med Biol. 1998;25:175–80.
72. Yaghoubi S, Barrio JR, Dahlbom M, et al. Human pharmacokinetic and dosimetry studies of [^{18}F]FHBG: a reporter probe for imaging herpes simplex virus type-1 thymidine kinase reporter gene expression. J Nucl Med. 2001;42:1225–34.
73. Yang DJ, Cherif A, Tansey W, et al. N, N-diethylfluoromethyltamoxifen: synthesis assignment of ^{1}H and ^{13}C spectra and receptor assay. Eur J Med Chem. 1992;27:919–24.
74. Yang D, Tewson T, Tansey W, et al. Halogenated analogs of tamoxifen: synthesis, receptor assay and inhibition of MCF7 cells. J Pharm Sci. 1992;81: 622–5.
75. Kim CG, Yang DJ, Kim EE, et al. Assessment of tumor cell proliferation using [^{18}F]fluorodeoxyadenosine and [^{18}F]fluoroethyluracil. J Pharm Sci. 1996;85(3):339–44.
76. Cherif A, Yang DJ, Tansey W, et al. Radiosynthesis and biodistribution studies of [F-18]fluoroadenosine and [I-131]-5-iodo-2′-O-methyl-uridine for the assessment of tumor proliferation rate. Pharm Res. 1995;12(9):128.
77. Yang D, Wallace S. High affinity tamoxifen derivatives and uses thereof. U.S. Patent no 5,192,525; 1993.
78. Yang D, Wallace S, Wright KC, et al. Imaging of estrogen receptors with PET using ^{18}F-fluoro analogue of tamoxifen. Radiology. 1992;182:185–6.
79. Yang DJ, Kuang L-R, Cherif A, et al. Synthesis of ^{18}F-alanine and ^{18}F-tamoxifen for breast tumor imaging. J Drug Target. 1993;1:259–67.
80. Yang DJ, Li C, Kuang L-R, et al. Imaging, biodistribution and therapy potential of halogenated tamoxifen analogues. Life Sci. 1994;55(1):53–67.
81. Yang DJ, Wallace S. High affinity halogenated tamoxifen derivatives and uses thereof. U.S. Patent no 5,219,548; 1993.
82. Inoue T, Kim EE, Wallace S, et al. Positron emission tomography using [^{18}F]fluorotamoxifen to evaluate therapeutic responses in patients with breast cancer: preliminary study. Cancer Biother Radiopharm. 1996;11(4):235–45.
83. Inoue T, Kim EE, Wallace S, et al. Preliminary study of cardiac accumulation of F-18 fluorotamoxifen in patients with breast cancer. Clin Imaging. 1997;21(5): 332–6.
84. Hanson RN, Seitz DE. Tissue distribution of the radiolabeled antiestrogen [^{125}I]iodotamoxifen. Int J Nucl Med Biol. 1982;9:105–7.
85. Ram S, Spicer LD. Radioiodination of tamoxifen. J Label Compd Radiopharm. 1989;27:661–8.
86. Kangas L, Nieminen A-L, Blanco G, et al. A new triphenylethylene, FC-1157a, antitumor effects. Cancer Chemother Pharmacol. 1986;17:109–13.
87. Kallio S, Kangas L, Blanco G, et al. A new triphenylethylene, FC-1157a, hormonal effects. Cancer Chemother Pharmacol. 1986;17:103–8.
88. Kawai G, Yamamoto Y, Kamimura T, et al. Conformational rigidity of specific pyrimidine residues in tRNA arises from posttranscriptional modifications that enhance steric interaction between the base and the 2′-hydroxyl group. Biochemistry. 1992;31:1040–5.

89. Uesugi S, Kaneyasu T, Ikehara M. Synthesis and properties of ApU analogues containing 2′-halo-2′-deoxyadenosine. Effect of 2′ substituents on oligonucleotide conformation. Biochemistry. 1982;21:5870–7.
90. Ikehara M, Miki H. Studies of nucleosides and nucleotides. Cyclonucleosides. Synthesis and properties of 2′-halogeno-2′-deoxyadenosines. Chem Pharm Bull. 1978;26:2449–53.
91. Inubushi M, Wu JC, Gambhir SS, et al. Positron-emission tomography reporter gene expression imaging in rat myocardium. Circulation. 2003;107(2):326–32.
92. Tjuvajev JG, Doubrovin M, Akhurst T, et al. Comparison of radiolabeled nucleoside probes (FIAU, FHBG, and FHPG) for PET imaging of HSV1-tk gene expression. J Nucl Med. 2002;43(8):1072–83.